Supporting Information

Cu and P co-doped bon for enhanced oxygen reduction reaction in zinc-air batteries

Experiments

Chemicals

All chemicals were used without further purification. Copper acetate monohydrate ($C_4H_6CuO_4 \cdot H_2O$, Macklin), Zinc acetate ($C_4H_6O_4Zn$, Macklin), Phytic acid solution ($C_6H_{18}O_{24}P_6$, Aladdin), Melamine ($C_3H_6N_6$, Aladdin), Potassium hydroxide (KOH, Aladdin), Ethyl Alcohol (CH_3CH_2OH, Chron chemicals), Sulfuric acid (H_2SO_4, Hushi).

Synthesis of Cu-PA-Zn

Firstly, 3.67g zinc acetate was poured into 33.3 mL deionized water. 3.6 ml 70% phytic acid solution was added in 16.7 ml deionized water and 20 mg copper acetate monohydrate was added and stirred. The above two solution was dropwise mixed under stirring, and reacted for 2 h. After centrifugation and washing, solid substance was collected by drying overnight in a vacuum oven(noted as Cu-PA-Zn).

Syntheses of PA-Zn and PA-Zn(Cu)

Similar to the preparation process of Cu-PA-Zn, PA-Zn was obtained without the addition of copper acetate monohydrate. The PA-Zn was then dispersed in 6 mL of ethyl alcohol containing 20 mg copper acetate monohydrate, followed by continuous grinding until the mixture was completely dry, the PA-Zn(Cu) sample was obtained.

Synthesis of Cu-P-N-C

Cu-PA-Zn with 0.5 g and melamine with 4 g were homogeneous mixed by grind. The obtained substance was annealed in a tube furnace with an argon atmosphere. The heating process is: from room temperature to 550 °C(5 °C/min) and maintained 1 hour; subsequently, from 550 °C to 950 °C(5 °C/min) and maintained 2 hour, then cooled down. The sample was etched in a 0.5 M H_2SO_4 at 80°C and 6 hours. The Cu-P-N-C catalyst was prepared by a second annealing process at 950°C for 2 hours,

Similarly, the Cu-P-N-C(Cm) catalyst was prepared by pyrolyzing the mixture of PA-Zn(Cu) and melamine; P-N-C catalyst was fabricated without copper acetate monohydrate.

Electrochemical Measurements

To test ORR activity, CHI 760E station, Hg/HgO reference electrode, glassy carbon working electrode, and carbon rod counter electrode were employed. The 0.1 M KOH was used as electrolytes. The catalyst ink was prepared by sonicating the mixture of carbon catalyst(5mg) and 1 ml of nafion/isopropanol (0.2 wt% Nafion). The working electrode was prepared through dropping catalyst ink (20 μL) over glassy carbon electrode(catalyst loading: 0.5 $mg \cdot cm^{-2}$).

The cyclic voltammetry (CV) and linear scanning voltammetry (LSV) with 1600 rpm are conducted in N_2/O_2-saturated 0.1 M KOH (10 $mV \cdot s^{-1}$). The hydrogen peroxide yield and electron transfer number (n) are obtained by RRDE technology.

$H_2O_2\ (\%) = 200 I_r\ (N I_d + I_r)^{-1}$ I_d: disk current; I_r: ring current

$n = 4\ I_d\ (I_d + I_r N^{-1})^{-1}$ N: ring collection efficiency

Zn-air Battery

The catalyst was coated on hydrophobic carbon paper(1 $mg \cdot cm^{-2}$) , as air cathode. The zinc plate was polished and washed, as anode. The electrolyte is 6 M KOH solution. The 760E workstation and NEWARE system was employed to test the assembled Zn-air battery.

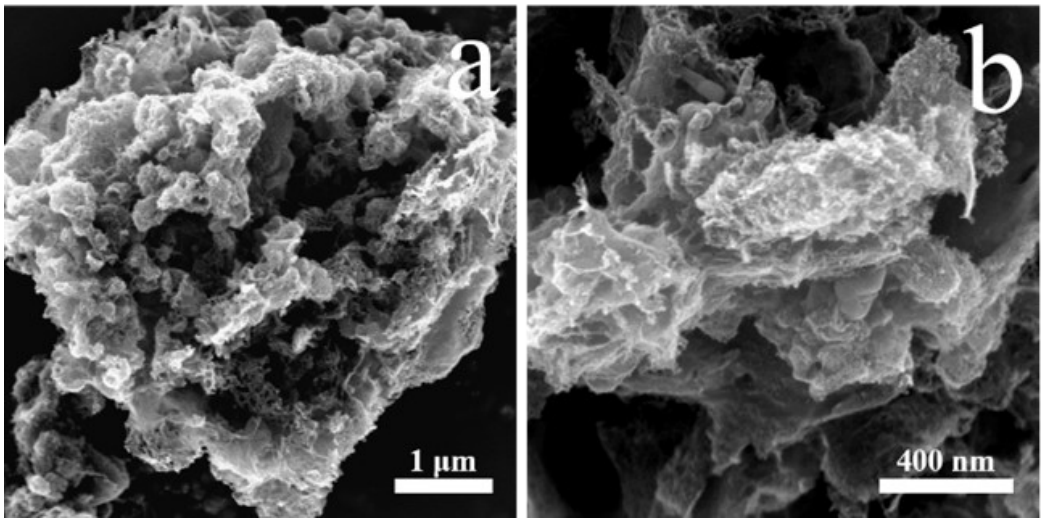

Figure S1. SEM images of P-N-C.

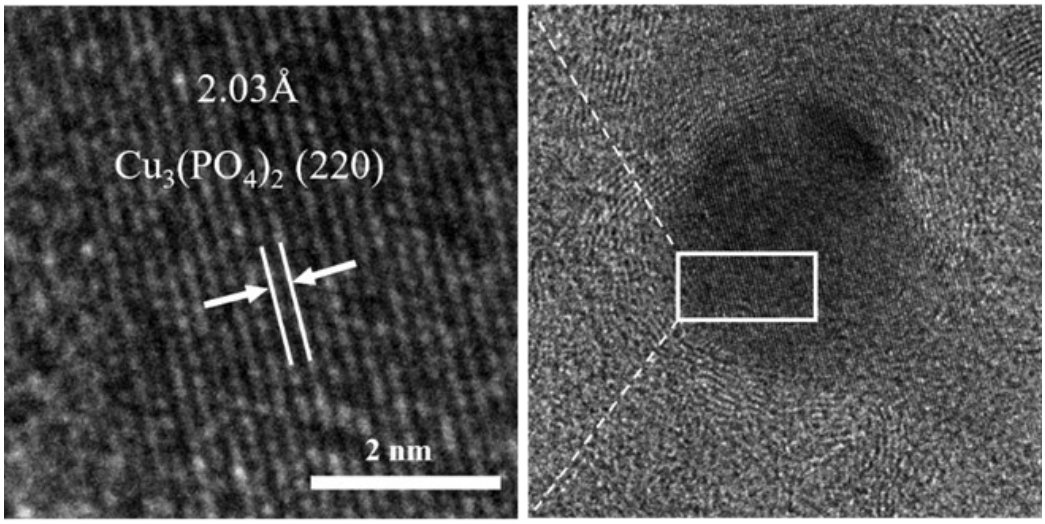

Figure S2. High-resolution TEM (HRTEM) images of Cu-P-N-C.

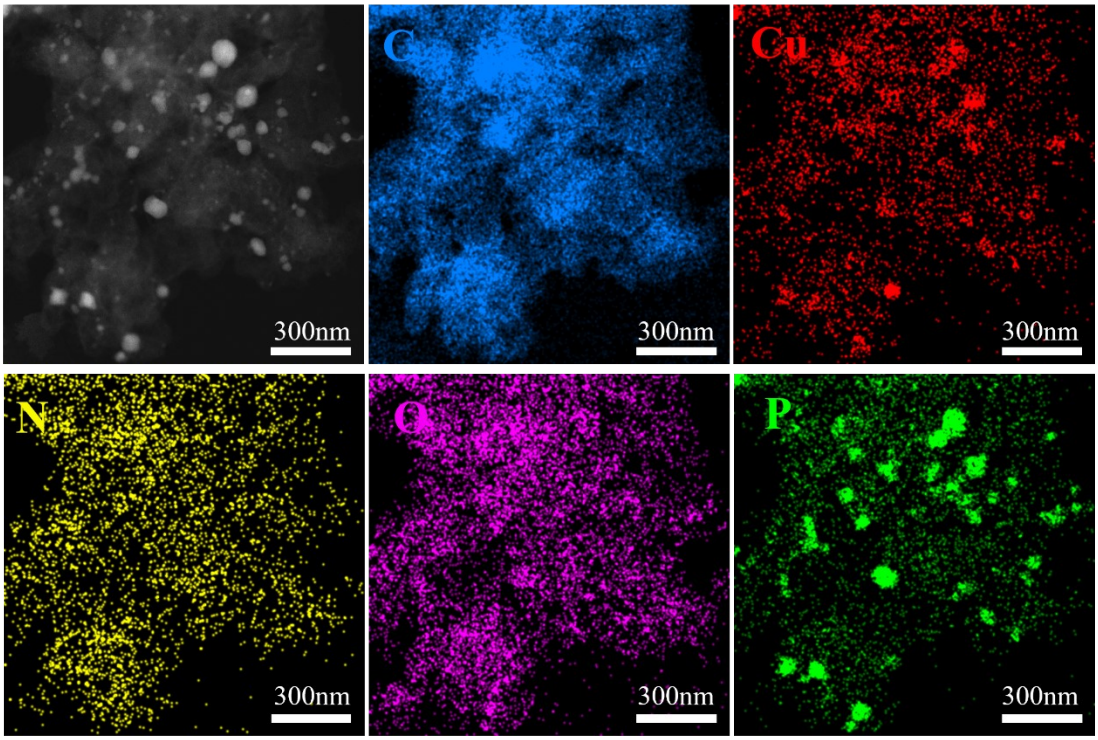

Figure S3. HAADF image and elemental mapping of Cu-P-N-C (Cm).

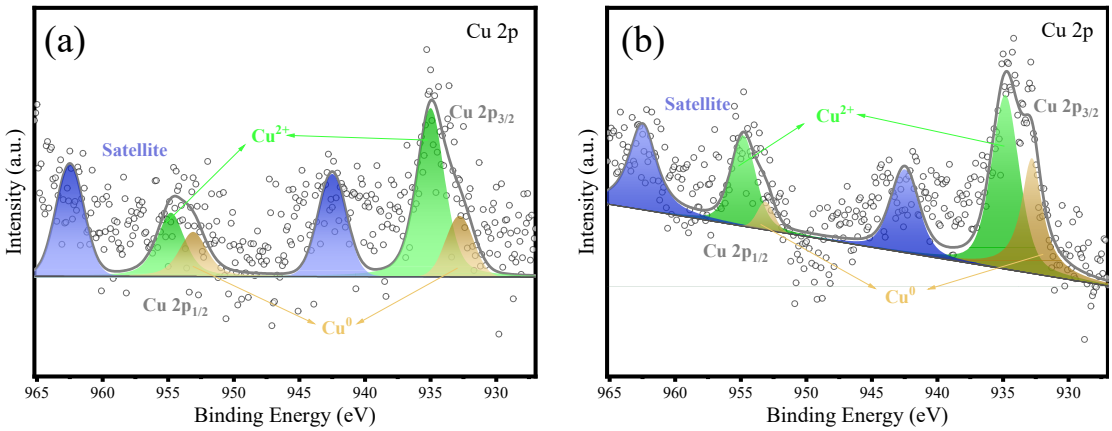

Figure S4. Cu 2p XPS spectra of (a) Cu-P-N-C and (b) Cu-P-N-C(Cm).

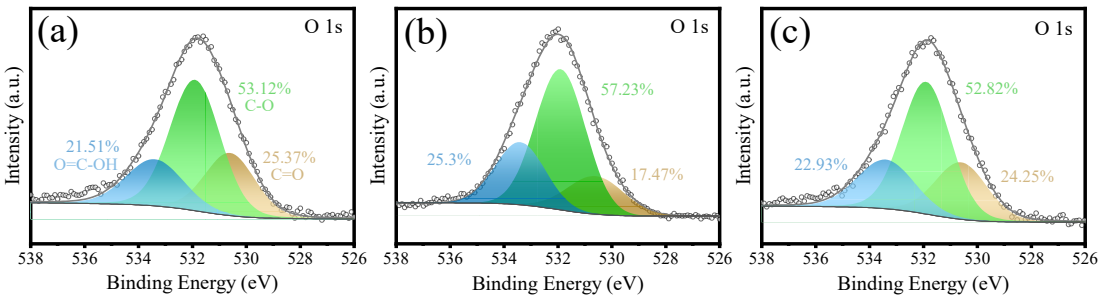

Figure S5. O 1s XPS spectra of (a) Cu-P-N-C, (b) Cu-P-N-C(Cm) and (c) P-N-C.

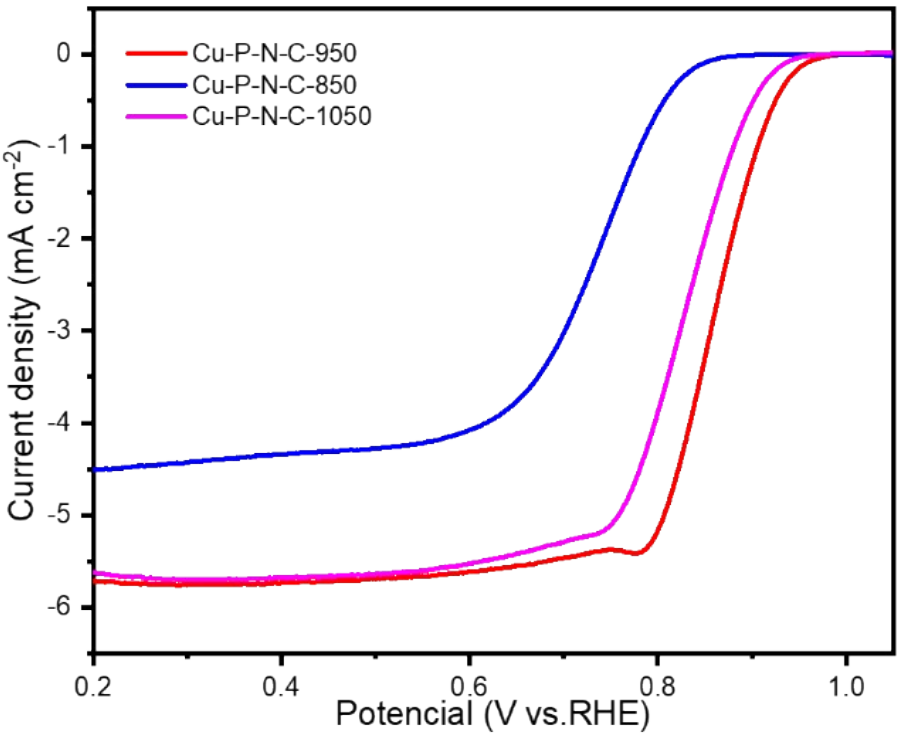

Figure S6. LSV curves of catalysts at different temperatures.

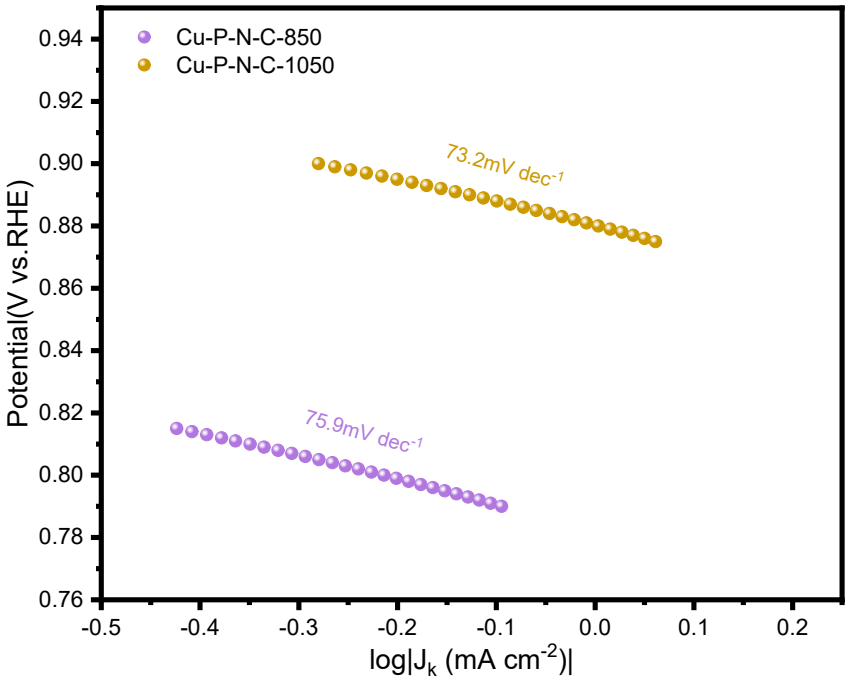

Figure S7. Tafel curves of P-N-C-850 and P-N-C-1050.

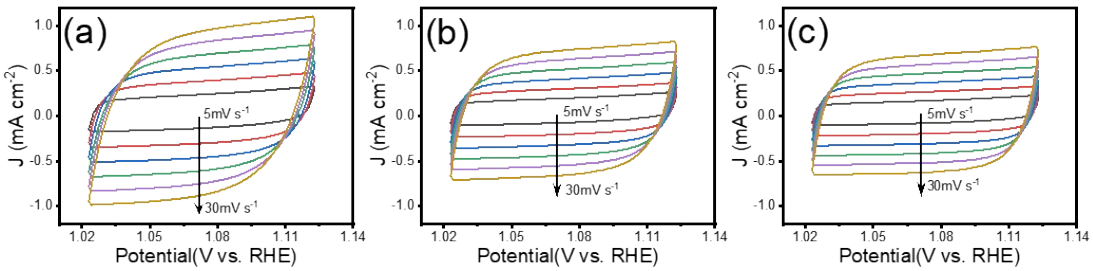

Figure S8. CV curves at various scan rates of (a) Cu-P-N-C, (b) Cu-P-N-C(Cm) and (c) P-N-C in 0.1 M KOH electrolyte.

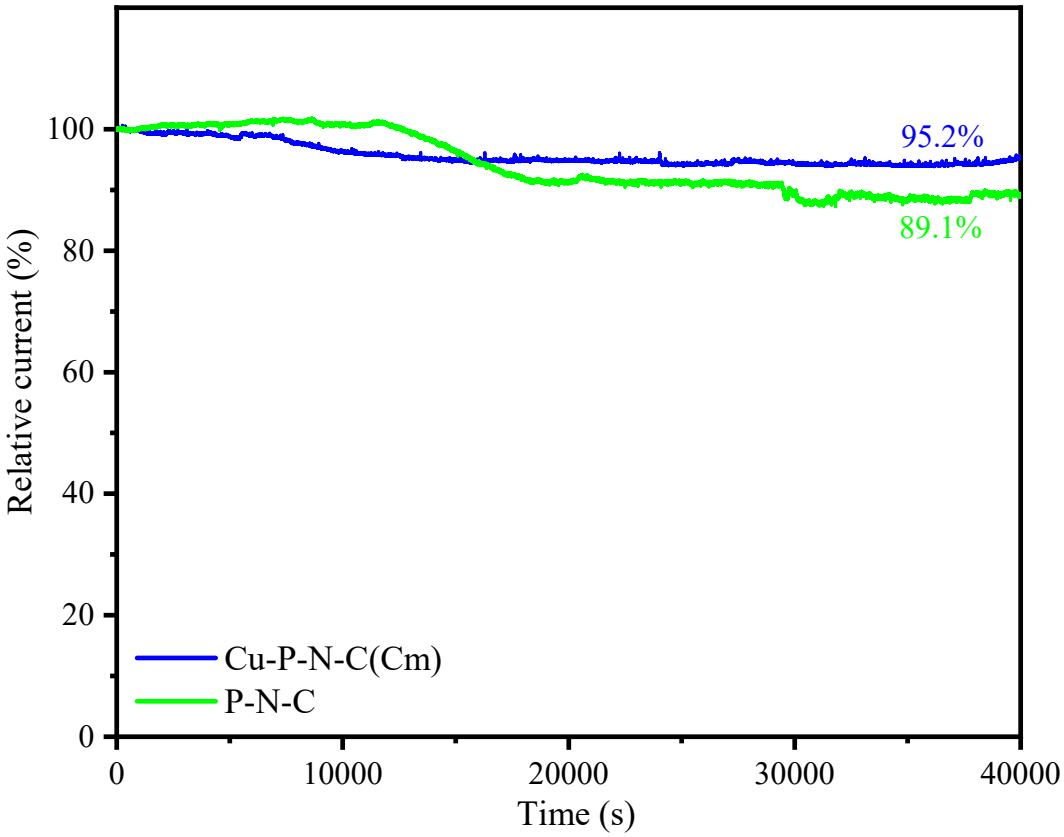

Figure S9. Chronoamperometric response curves of Cu-P-N-C(Cm) and P-N-C

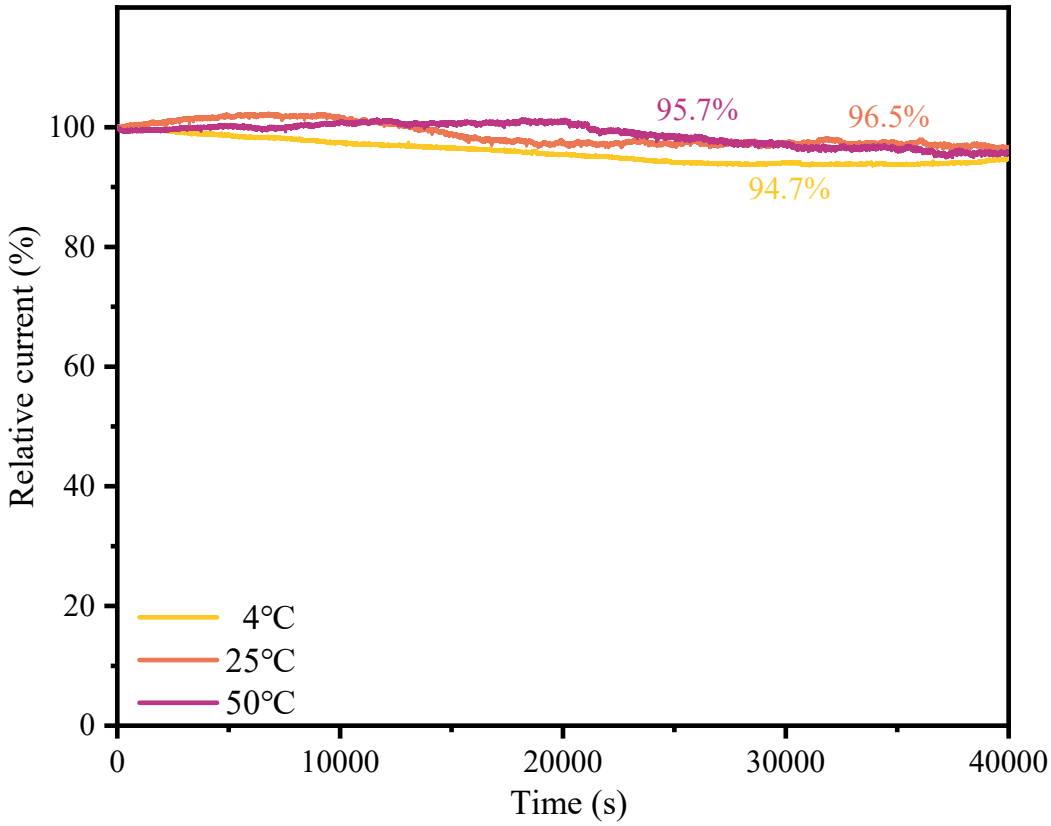

Figure S10. Chronoamperometric response curves of Cu-P-N-C in O_2-saturated 0.1 M KOH solution at 4°C, 25°C, and 50°C.

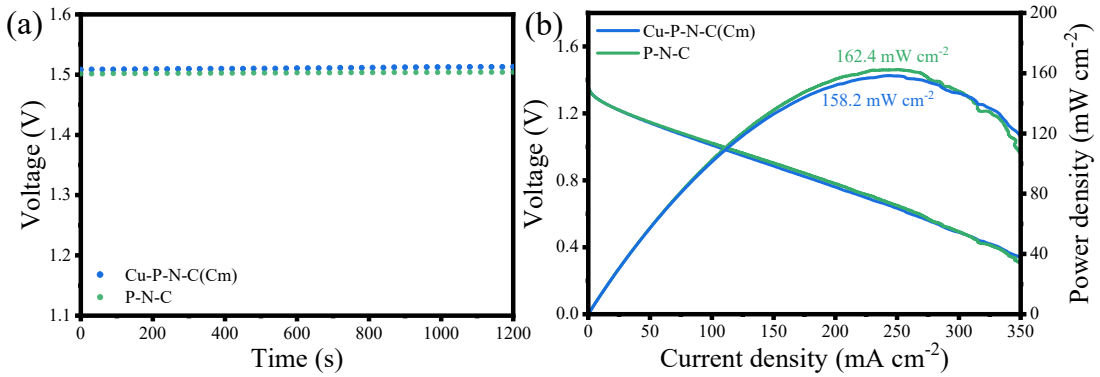

Figure S11. (a) Open circuit voltage. (b) Polarization and power density curves of Cu-P-N-C(Cm) and P-N-C based ZABs in 6M KOH.

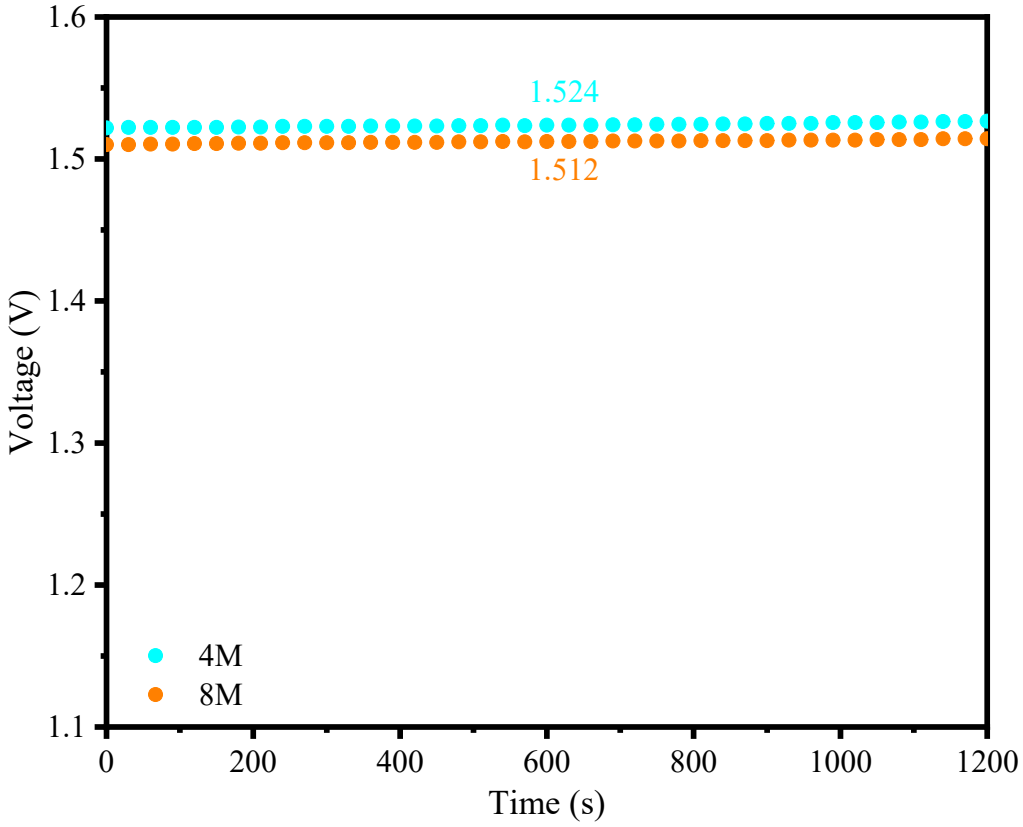

Figure S12. (a) Open circuit voltage. (b) Voltage-Time discharge curve of Cu-P-N-C based ZABs with electrolyte concentrations.

Table S1. Comparison of ORR performances in alkaline electrolyte among recently reported the P and N co-doped ORR catalysts.

Catalyst	E_0 (V vs. RHE)	$E_{1/2}$ (V *vs.* RHE)	J_d (mA cm^{-2})	Ref.
Cu-P-N-C	1.02	0.86	5.72	This work
P-N-C	0.99	0.851	5.51	This work
Co-N-$P_{1.5}$-MC	1.02	0.84	5.51	1
2.5Co_2P-NPC-CeO_2	0.88	0.827	5.24	2
CNP-act825-4	0.925	0.838	4.53	3
PA-SS 900	0.96	0.82	4.47	4
CNFP-act	0.931	0.867	5.10	5
NPDC-1.09	0.94	0.84	6.01	6
N,P-SiCDC1	0.9	0.79	---	7
M-PNC-1000	0.95	0.84	5.3	8
P-Fe_3Co_1@NC/CNTs	0.860	0.802	5.29	9
SWCNT@NPC	---	0.85	---	10
FeCoP/C	---	0.849	---	11
$Co(PO_3)_2$/NC	0.906	0.780	5.062	12
BP-CN-c	---	0.84	5.34	13
PANI-Fe/PA-N1050	---	0.84	4.4	14
Fe-N/P-C-700	0.941	0.867	5.66	15
NPSP- 900	---	0.83	---	16

Table S2. The comparison of zinc-air battery performance with Cu-P-N-C and the recently reported carbon catalysts as cathodes

Catalyst	Open voltage (V)	Peak power density ($mW \cdot cm^{-2}$)	Specific capacity ($mAh \cdot g^{-1}$)	Ref.
Cu-P-N-C	1.53	164.5	807 (20 mA cm^{-2})	This work
S-VN/Co/NS-MC	1.49	195.7	815.7 (20)	17
CNT@SAC-Co/NCP	1.45	172	---	18
WN-Ni@pDC-750-0.02	1.40	165	748 (10)	19
CoP@NC-Ru	1.51	175	780 (50)	20
CeO_2–Fe_2N/NFC_{-2}	1.43	133	---	21
J-CeO_2/ZCS	1.44	168.7	785.9 (10)	22
Fe-N_4@NC-PCSs	1.465	207	819 (10)	23
CoS_2 YSS@NC-0.5	1.4	202	772.5 (10)	24
Co/CoN_4PCF	1.47	196	805 (10)	25
CoNi@NC	1.45	168.8	870 (10)	26
CoN/MnO@NC	1.56	153	718 (10)	27
Cu-Co/NC	1.45	295.9	694 (20)	28

References

1. Cai S, Meng Z, Li G, et al. Nitrogen doped porous carbon-based bifunctional oxygen electrocatalyst with controllable phosphorus content for zinc-air battery. *Nano Res.*, 2023, 16(4): 5887-5893.

2. Wang X, Xu J, Zhi M, et al. Synthesis of Co_2P nanoparticles decorated nitrogen, phosphorus Co-doped Carbon-CeO_2 composites for highly efficient oxygen reduction. *J. Alloy. Compd.*, 2019, 801: 192-198.

3. Takada R, Shu Y, Taniguchi Y, et al. Facile synthesis of carbon co-doped with nitrogen and phosphorus as metal-free electrocatalyst with precisely controlled pore structure and dual heteroatoms for oxygen reduction reaction. *Carbon*, 2024, 218: 118719.

4. Zheng F Y, Li R, Ge S, et al. Nitrogen and phosphorus co-doped carbon networks derived from shrimp shells as an efficient oxygen reduction catalyst for microbial fuel cells. *J. Power Sources*, 2020, 446: 227356.

5. Takada R, Narimatsu K, Taniguchi Y, et al. Nitrogen, fluorine, and phosphorus tri-doped porous carbon with high electrical conductivity as an excellent metal-free electrocatalyst for oxygen reduction reaction. *ChemCatChem*, 2024: e202400749.

6. Han L, Cui X, Liu Y, et al. Nitrogen and phosphorus modification to enhance the catalytic activity of biomass-derived carbon toward the oxygen reduction reaction. *Sustain. Energ. Fuels*, 2020, 4(6): 2707-2717.

7. Palm I, Kibena-Poldsepp E, Mäeorg U, et al. Silicon carbide-derived carbon electrocatalysts dual doped with nitrogen and phosphorus for the oxygen reduction reaction in an alkaline medium. *Electrochem. Commun.*, 2021, 125: 106976.

8. Xia W, Hunter M A, Wang J, et al. Highly ordered macroporous dual-element-doped carbon from metal–organic frameworks for catalyzing oxygen reduction. *Chem. Sci.*, 2020, 11(35): 9584-9592.

9. Zhang R, Wang Z, Zhu L, et al. Phosphorus modification of cobalt–iron nanoparticles embedded in a nitrogen-doped carbon network for oxygen reduction reaction. *RSC Adv.*, 2021, 11(16): 9450-9458.

10. Li J C, Hou P X, Cheng M, et al. Carbon nanotube encapsulated in nitrogen and phosphorus co-doped carbon as a bifunctional electrocatalyst for oxygen reduction and evolution reactions. *Carbon*, 2018, 139: 156-163.

11. Zhao R, Ni B, Wu L, et al. Carbon-based iron-cobalt phosphate FeCoP/C as an effective ORR/OER/HER trifunctional electrocatalyst. *Colloid Surf. A-Physicochem. Eng. Asp.*, 2022, 635: 128118.

12. Xu L H, Zhang S L, Guo S Y, et al. ATMP derived cobalt-metaphosphate complex as highly active catalyst for oxygen reduction reaction. *J. Catal.*, 2020, 387: 129-137.

13. Wang X, Raghupathy R K M, Querebillo C J, et al. Interfacial covalent bonds regulated electron-deficient 2D black phosphorus for electrocatalytic oxygen reactions. *Adv. Mater.*, 2021, 33(20): 2008752.

14. Liu J, Zhu Y, Du F, et al. Iron/nitrogen/phosphorus co-doped three-dimensional porous carbon as a highly efficient electrocatalyst for oxygen reduction reaction. *J. Electrochem. Soc.*, 2019, 166(13): F935.

15. Yuan K, Lützenkirchen-Hecht D, Li L, et al. Boosting oxygen reduction of single iron active sites via geometric and electronic engineering: nitrogen and phosphorus dual coordination. *J. Am. Chem. Soc.*, 2020, 142(5): 2404-2412.

16. Lu L, Yu J, Wu Z, et al. Shaddock peel derived nitrogen and phosphorus dual-doped hierarchical porous carbons as high-performance catalysts for oxygen reduction reaction. *Int. J. Hydrog. Energy*, 2019, 44(49): 26982-26991.

17. Deng D, Zhang H, Wu J, et al. Electronic structure and spin state regulation of vanadium nitride via a sulfur doping strategy toward flexible zinc-air batteries. *J. Energy Chem.*, 2024, 89: 239-249.

18. Li J C, Meng Y, Zhang L, et al. Dual-phasic carbon with Co single atoms and nanoparticles as a bifunctional oxygen electrocatalyst for rechargeable Zn-air batteries. *Adv. Funct. Mater.*, 2021, 31(42): 2103360.

19. Du Y, Chen W, Zhong Z, et al. Bifunctional oxygen electrocatalysts with WN@ Ni nanostructures implanted on N-doped carbon nanorods for rechargeable Zn-Air batteries. *J. Alloy. Compd.*, 2023, 960: 170789.

20. Kumar M M, Aparna C, Nayak A K, et al. Surface Tailoring-Modulated Bifunctional Oxygen Electrocatalysis with CoP for Rechargeable Zn–Air Battery and Water Splitting. *ACS Appl. Mater. Interfaces*, 2024, 16(3): 3542-3551.

21. Wang M, Ren J, Wang H, et al. Boosting oxygen evolution electrocatalysis via CeO_2 engineering on Fe_2N nanoparticles for rechargeable Zn-air batteries. *Nanoscale*, 2023, 15(18): 8217-8224.

22. Zhang J, Dong X, Wang G, et al. Interfacial engineering-induced Janus heterostructures with enhanced electronic regulation for efficient oxygen electrocatalysis in rechargeable Zn-air batteries. *Appl. Catal. B-Environ.*, 2024, 342: 123459.

23. Li C, Yuan M, Liu Y, et al. Graphite-N modified single Fe atom sites embedded in hollow leaf-like nanosheets as air electrodes for liquid and flexible solid-state Zn-air batteries. *Chem. Eng. J.*, 2023, 477: 146988.

24. Xie J, Liu J, Liu B, et al. Yolk shell-structured pyrite-type cobalt sulfide grafted by nitrogen-doped carbon-needles with enhanced electrical conductivity for oxygen electrocatalysis. *Chin. Chem. Lett.*, 2024, 35(7): 109236.

25. Chen Y, Wu Y, Li L, et al. Hierarchical wood cells impose well-textured carbon nanotubes with cobalt single atoms: Bioinspired construction and application in zinc-air battery. *Chem. Eng. J.*, 2023, 475: 145993.

26. Zhou Q, Miao S, Xue T, et al. Nitrogen-doped porous carbon encapsulates multivalent cobalt-nickel as oxygen reduction reaction catalyst for zinc-air battery. *J. Colloid Interface Sci.*, 2023, 648: 511-519.

27. Niu Y, Jiang G, Gong S, et al. Engineering of heterointerface of ultrathin carbon nanosheet-supported CoN/MnO enhances oxygen electrocatalysis for rechargeable Zn-air batteries. *J. Colloid Interface Sci.*, 2024, 656: 346-357.

28. Li Z, Ji S, Wang C, et al. Geometric and Electronic Engineering of Atomically Dispersed Copper-Cobalt Diatomic Sites for Synergistic Promotion of Bifunctional Oxygen Electrocatalysis in Zinc-Air Batteries. *Adv. Mater.*, 2023, 35(25): 2300905.